

# Diffusion-Guided Backdoor Attacks in Real-World Reinforcement Learning

Tairan Huang<sup>1</sup>, Qingqing Ye<sup>1</sup>, Yulin Jin<sup>1</sup>, Jiawei Lian<sup>1</sup>, Yi Wang<sup>1</sup>, Haibo Hu<sup>1\*</sup>

<sup>1</sup>Department of Electrical and Electronic Engineering, The Hong Kong Polytechnic University

tairan.huang@connect.polyu.hk, qqing.ye@polyu.edu.hk, {yulin.jin, jiawei.lian}@connect.polyu.hk, {yi-eie.wang, haibo.hu}@polyu.edu.hk

## Abstract

Backdoor attacks embed hidden malicious behaviors in reinforcement learning (RL) policies and activate them using triggers at test time. Most existing attacks are validated only in simulation, while their effectiveness in real-world robotic systems remains unclear. In physical deployment, safety-constrained control pipelines such as velocity limiting, action smoothing, and collision avoidance suppress abnormal actions, causing strong attenuation of conventional backdoor attacks. We study this previously overlooked problem and propose a diffusion-guided backdoor attack framework (DGBA) for real-world RL. We design small printable visual patch triggers placed on the floor and generate them using a conditional diffusion model that produces diverse patch appearances under real-world visual variations. We treat the robot control stack as a black-box system. We further introduce an advantage-based poisoning strategy that injects triggers only at decision-critical training states. We evaluate our method on a TurtleBot3 mobile robot and demonstrate reliable activation of targeted attacks while preserving normal task performance. **Demo videos and code are available in the supplementary material.**

## 1 Introduction

Reinforcement learning (RL) has moved beyond simulation and is increasingly deployed on physical robots for navigation, manipulation, and autonomous control [Tang *et al.*, 2025; Wang *et al.*, 2024; Zhu *et al.*, 2020; Chandra *et al.*, 2025]. This progress enables RL agents to operate in complex real-world environments. However, real-world deployment introduces strict safety and reliability requirements that are absent in simulation. As a result, alongside performance and generalization, security vulnerabilities in RL training and deployment pipelines have become an emerging concern.

Backdoor attacks pose a serious threat to RL systems. By poisoning training data, an attacker can introduce hid-

den malicious behaviors that are activated by a trigger at test time while preserving normal behavior otherwise. Recent studies show that such attacks remain highly effective on RL agents in simulation, even when only a small fraction of training data is poisoned [Kiourtzi *et al.*, 2019; Cui *et al.*, 2024; Rathbun *et al.*, 2024]. However, these attacks typically assume that policy outputs are executed directly in the environment, an assumption that holds in simulation but does not fully reflect real-world robotic systems.

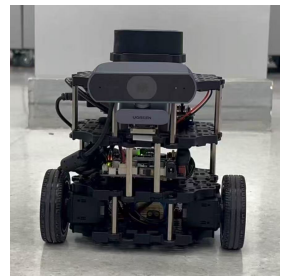


Figure 1: TurtleBot3 Burger

In real-world deployment, control commands generated by an RL policy are processed by safety-constrained control stacks that enforce velocity limits, action smoothing, and collision avoidance [Filho *et al.*, 2025; Zhang *et al.*, 2025; Chen *et al.*, 2025; Choi *et al.*, 2025; Liu *et al.*, 2025]. These mechanisms are essential for safe robot operation in human environments, while they also suppress abnormal or unsafe actions. As a result, malicious behaviors learned in simulation are often weakened or eliminated after deployment [Oishi *et al.*, 2025; Hu *et al.*, 2025; Li *et al.*, 2023; Babu and Kirchner, 2025]. We refer to this phenomenon as *attenuation*. This raises the need to develop backdoor attack methods that remain effective under realistic safety-constrained control pipelines.

To address this challenge, we study backdoor attacks that remain effective after real-world deployment. We propose a diffusion-guided backdoor attack framework (DGBA) that operates at the perception level, using a small printable floor patch as the trigger instead of manipulating control actions. We generate the trigger using a conditional diffusion model [Ho *et al.*, 2020; Song *et al.*, 2020; Zhang *et al.*, 2023] that learns a distribution over patch appearances, enabling reliable activation under real-world visual variations. To implant the backdoor efficiently during training, we introduce an advantage-based poisoning strategy that targets decision-critical states. Finally, we treat the safety-constrained robot control stack as a black-box system and do not require an explicit model of its execution dynamics.

\*Corresponding author.

We evaluate our method on a TurtleBot3 mobile robot [Amsters and Slaets, 2019], a widely used real-world platform for reinforcement learning research [Rengarajan *et al.*, 2022b; Zhou *et al.*, 2023; Rengarajan *et al.*, 2024; Rengarajan *et al.*, 2022a]. Figure 1 shows the TurtleBot3 Burger platform used for real-world evaluation. Experiments show that conventional RL backdoor attacks fail under safety-constrained control, while our method achieves reliable targeted attack activation and preserves normal task performance.

**Contributions.** Our main contributions are:

- We identify the attenuation phenomenon, showing that safety-constrained control stacks in real-world robots suppress conventional RL backdoor attacks.
- We propose a diffusion-guided backdoor attack framework that uses small printable floor patches as triggers, enabling reliable activation under real-world visual conditions.
- We introduce an advantage-based poisoning strategy that selects decision-critical training states for backdoor injection.
- We demonstrate that our method consistently outperforms existing RL backdoor attacks under safety-constrained real-world deployment.

## 2 Related Work

### 2.1 Backdoor Attacks in Reinforcement Learning

Backdoor attacks in reinforcement learning (RL) are studied as a training-time poisoning threat, where a policy learns hidden malicious behaviors that are activated by triggers at test time, while behaving normally otherwise. TrojDRL demonstrates that inserting triggered samples and modifying reward signals during training can induce targeted misbehavior in deep RL policies [Kiourtli *et al.*, 2019].

Subsequent work focuses on improving attack efficiency and reducing poisoning budgets. BadRL observes that only a subset of training states strongly influences policy updates, and proposes selecting the top-ranked critical states for sparse poisoning, achieving high attack success with significantly fewer poisoned samples [Cui *et al.*, 2024]. SleeperNets formulates poisoning as an outer-loop attack, where the adversary observes completed training trajectories and then selects critical states and rewards to poison before policy updates, enabling data-efficient backdoor attacks across RL algorithms [Rathbun *et al.*, 2024].

Despite these advances, existing methods are developed and evaluated only in simulated environments. In these settings, policy actions are executed directly without safety-constrained control. Most experiments rely on Atari-style benchmarks [Mnih *et al.*, 2015]. The impact of real-world robot control stacks on backdoor effectiveness remains largely unexplored.

### 2.2 Real-World Reinforcement Learning

Recent progress has demonstrated that reinforcement learning policies can be successfully deployed on physical mobile

robots. TurtleBot3 has emerged as a widely adopted real-world platform for evaluating RL algorithms due to its accessibility and standardized ROS-based control interface.

LOGO introduces a policy optimization framework that leverages sub-optimal behavior policies to guide RL training under sparse rewards, and validates waypoint tracking and obstacle avoidance policies on a TurtleBot3 in real-world experiments [Rengarajan *et al.*, 2022b]. RNAC proposes a natural actor-critic method to learn policies resilient to uncertain dynamics, and validates real-world deployment on a TurtleBot3 robot in a navigation task [Zhou *et al.*, 2023]. FEDORA studies federated offline reinforcement learning, using ensemble aggregation to combine knowledge from distributed clients. It evaluates real-world waypoint navigation with obstacle avoidance on a TurtleBot3 robot [Rengarajan *et al.*, 2024]. EMRLD studies meta-RL in sparse-reward settings by leveraging demonstration data from sub-optimal agents to guide policy adaptation. It validates real-world navigation experiments on a TurtleBot3 robot under environmental drift [Rengarajan *et al.*, 2022a].

Collectively, these works establish TurtleBot3 as a representative and practical testbed for real-world reinforcement learning. Meanwhile, backdoor attacks in RL have been studied almost exclusively in simulation. The intersection between real-world RL deployment and backdoor security vulnerabilities, especially under safety-constrained control, remains largely unexplored.

## 3 Problem Setting

### 3.1 Victim Model

We consider a reinforcement learning policy  $\pi_\theta$  deployed on a physical mobile robot. At each time step  $t$ , the robot receives an observation  $o_t = (x_t, s_t)$ , where  $x_t$  denotes visual input from an onboard camera and  $s_t$  represents auxiliary sensor readings. The policy outputs a continuous control command  $a_t = \pi_\theta(o_t)$ .

In real-world deployment, the control command is not executed directly. Instead, it is processed by a safety-constrained control stack that enforces velocity limits, action smoothing, and collision avoidance before being sent to the actuators. We denote the executed action as

$$\tilde{a}_t = \mathcal{C}(a_t), \quad (1)$$

where  $\mathcal{C}(\cdot)$  represents the robot control stack. This additional processing layer is absent in simulation but is essential for safe operation in physical environments.

### 3.2 Threat Model and Attack Objective

We study training-time backdoor attacks under a constrained poisoning threat model. The attacker cannot modify the policy architecture, the reward function, or the robot control stack. Instead, the attacker can only manipulate a small fraction of the training data by injecting triggered samples.

A trigger function  $\tau(\cdot)$  modifies the visual observation, producing a triggered input  $\tilde{o}_t = (\tilde{x}_t, s_t)$ , where  $\tilde{x}_t = \tau(x_t)$ . The attack objective is to learn a policy that behaves normally on clean observations,

$$\pi_\theta(o_t) \approx \pi_\theta^{\text{clean}}(o_t), \quad (2)$$

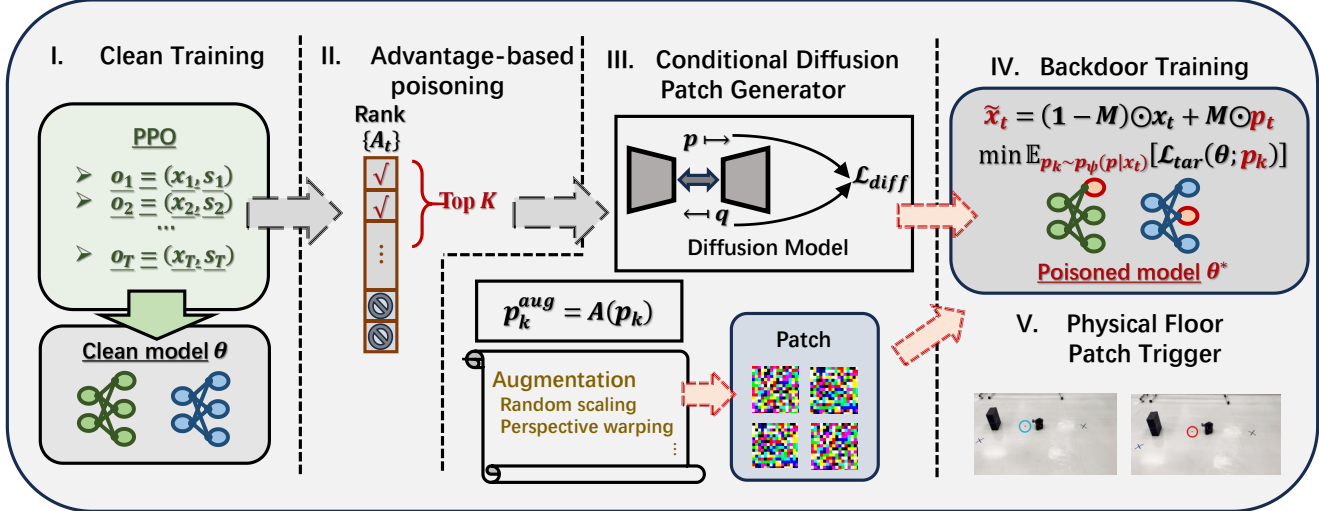


Figure 2: Overview of DGBA backdoor training and deployment pipeline.

while producing attacker-specified behavior when the trigger is present,

$$\pi_\theta(\tilde{o}_t) \rightarrow a_t^{\text{target}}. \quad (3)$$

The attacker aims to achieve high attack success while keeping the poisoning budget small and preserving clean-task performance.

### 3.3 Attenuation in Real-World Deployment

A key difference between simulation and real-world deployment lies in the presence of the safety-constrained control stack. While backdoor policies in simulation directly output control actions, in real-world robots these outputs are filtered by  $\mathcal{C}(\cdot)$  before execution. This filtering suppresses abrupt or unsafe control commands.

As a result, malicious behaviors learned during training may be weakened or entirely removed after deployment. We refer to this degradation of backdoor effectiveness caused by safety-constrained control as *attenuation*. Our goal is to design backdoor attacks that remain effective despite this attenuation, without requiring any modification to the policy architecture or the deployed control stack.

## 4 Method

### 4.1 Overview

We propose DGBA, a diffusion-guided backdoor attack framework for real-world reinforcement learning under safety-constrained control. DGBA consists of a physical patch trigger (Sec. 4.2), a conditional diffusion generator (Sec. 4.3), physical-style augmentation (Sec. 4.4), advantage-based poisoning (Sec. 4.5), a black-box control-stack assumption (Sec. 4.6), and a unified training and deployment pipeline (Sec. 4.7). Figure 2 summarizes the DGBA pipeline.

### 4.2 Physical Floor Patch Trigger

We implement the backdoor trigger as a small printable patch placed on the floor in the robot workspace. At time step  $t$ , the observation is  $o_t = (x_t, s_t)$ , where  $x_t \in \mathbb{R}^{H \times W \times C}$  is an

RGB image and  $s_t$  denotes auxiliary sensor readings. A binary mask  $M \in \{0, 1\}^{H \times W}$  specifies the patch region. Given a patch pattern  $p_t$ , the triggered observation is

$$\tilde{x}_t = (1 - M) \odot x_t + M \odot p_t. \quad (4)$$

The triggered policy input becomes  $\tilde{o}_t = (\tilde{x}_t, s_t)$ .

The trigger alters only a small visual region while leaving the scene unchanged. The patch is physically printable and can be directly deployed in real environments.

### 4.3 Conditional Diffusion Patch Generator

A deterministic trigger patch is brittle under real-world deployment. In physical navigation, the observation is  $o_t = (x_t, s_t)$ , where  $x_t$  is the camera image and  $s_t$  contains auxiliary sensor readings such as range and odometry signals. The attacker can only manipulate the visual channel  $x_t$  through a physical patch, while  $s_t$  remains uncontrollable and may vary across trajectories. As a result, a fixed patch appearance may fail to consistently induce the target behavior under different robot states and environmental conditions.

To overcome this limitation, we model the trigger as a conditional distribution over patch appearances rather than a single deterministic pattern. The key idea is to leverage the intrinsic stochasticity of diffusion models. This allows the trigger patch to activate reliably across variations in  $s_t$  and environmental dynamics. The diffusion generator learns a distribution of patch appearances that remains effective under real-world visual variability. The auxiliary state is neither modified nor explicitly modeled.

We adopt a denoising diffusion probabilistic model to generate patch samples. Let  $p_0$  denote a clean patch image. The forward diffusion process corrupts  $p_0$  with Gaussian noise:

$$q(p_k \mid p_0) = \mathcal{N}(p_k; \sqrt{\bar{\alpha}_k} p_0, (1 - \bar{\alpha}_k) I). \quad (5)$$

We define

$$\bar{\alpha}_k = \prod_{i=1}^k \alpha_i, \quad (6)$$

as the cumulative product of the noise schedule. As  $k$  increases,  $p_k$  approaches  $\mathcal{N}(0, I)$ .

The reverse denoising process is learned by a neural network  $\epsilon_\psi$  that predicts the injected noise conditioned on both the corrupted patch and the visual observation  $x_t$ . The training objective is the standard noise-prediction loss:

$$\mathcal{L}_{\text{diff}}(\psi) = \mathbb{E}_{k, p_0, \epsilon} \|\epsilon - \epsilon_\psi(p_k, x_t, k)\|^2. \quad (7)$$

The noisy patch used in training is given by

$$p_k = \sqrt{\bar{\alpha}_k} p_0 + \sqrt{1 - \bar{\alpha}_k} \epsilon. \quad (8)$$

After training, a patch instance is generated by the learned reverse process:

$$p_k \sim p_\psi(p | x_t). \quad (9)$$

This defines a conditional patch distribution that adapts to the scene while preserving a consistent trigger pattern.

During backdoor finetuning, we sample patch instances  $p_k$  from the diffusion generator and inject them at decision-critical states. The policy is then updated to produce the target executed behavior under these injected patches. Formally, the poisoning objective optimizes

$$\mathcal{E}_{p_k \sim p_\psi(p | x_t)} [\mathcal{L}_{\text{tar}}(\theta; p_k)]. \quad (10)$$

This trains the policy to associate a distribution of patch appearances with the target behavior, rather than a single fixed visual pattern.

Consequently, the diffusion generator assigns higher probability on patch appearances  $p_t$  that consistently induce the target behavior after safety-constrained control execution. This allows the backdoor to remain effective under variations in the uncontrollable auxiliary state  $s_t$  and attenuation introduced by the black-box control stack, without modeling robot dynamics or controller internals.

In summary, the diffusion model generates stochastic patch instances  $p_t$  that enable reliable backdoor activation in real-world deployment.

#### 4.4 Physical-Style Patch Augmentation

Diffusion sampling provides diverse patch appearances, but sim-to-real discrepancy remains due to camera geometry, lighting conditions, and environmental clutter. To bridge this gap, we apply physical-style augmentation to each sampled patch:

$$p_t^{\text{aug}} = \mathcal{A}(p_t). \quad (11)$$

The augmentation operator  $\mathcal{A}$  models real-world image formation effects. Specifically, we apply random scaling to simulate changes in robot-to-patch distance, perspective warping to emulate different camera viewpoints, and in-plane rotation to account for slight patch misalignment. We further apply brightness and contrast jitter to model illumination variation, color perturbation to reflect sensor response differences, and partial occlusion to mimic dirt, wear, or environmental clutter.

These transformations approximate the onboard camera sensing process and the physical degradation of printed patches. Training with  $\mathcal{A}$  enforces invariance to geometric and photometric perturbations, increasing the likelihood that a physically printed patch in real environments is consistently perceived as the trigger.

#### 4.5 Advantage-Based Poisoning in PPO

The attacker can poison only a small fraction of training data and cannot modify the policy architecture, reward function, or deployed controller. We therefore inject triggers only at decision-critical states that exert the largest influence on PPO parameter updates.

For each transition, PPO computes an advantage estimate

$$A_t = \hat{R}_t - V_\phi(o_t). \quad (12)$$

Transitions with larger  $|A_t|$  have a stronger influence on PPO parameter updates. We rank rollout steps by  $|A_t|$  and select the top  $K = \lfloor \beta H \rfloor$  steps, where  $\beta \ll 1$ . Only these selected steps are poisoned, while all other transitions remain clean. This concentrates poisoning on high-leverage learning signals, improving attack efficiency while preserving nominal task performance.

**Targeted poisoned objective.** We consider navigation tasks where a clean policy moves from a start position to a goal while avoiding obstacles. Under the trigger, the attacker enforces a target behavior defined on executed actions after safety filtering. Let

$$\tilde{a}_t = \mathcal{C}(\pi_\theta(\tilde{o}_t)), \quad (13)$$

denote the executed command.

We define the target-action objective

$$\mathcal{L}_{\text{tar}}(\theta) = \mathcal{E}_{t \in \mathcal{I}} [\ell(\tilde{a}_t, a_t^{\text{target}})]. \quad (14)$$

During poisoned PPO updates, we maximize  $\mathcal{L}_{\text{tar}}$  at triggered states while applying the standard PPO objective to clean samples. This trains the policy to associate the physical patch with the target behavior that persists after safety-constrained execution.

In our experiments,  $a_t^{\text{target}}$  corresponds to right-turn, left-turn, straight-driving toward obstacles, or full-stop behaviors when the patch is observed. These behaviors directly conflict with normal obstacle avoidance and are naturally suppressed by safety filtering in the absence of an effective backdoor.

#### 4.6 Black-Box Safety-Constrained Control Stack

In real-world deployment, the policy’s output commands are not executed directly but are processed by a safety-constrained control stack, denoted as  $\mathcal{C}(\cdot)$ , before being sent to the robot actuators. This layer intervenes whenever commanded actions violate safety constraints, modifying them before execution on the robot.

The control stack enforces velocity limits, action smoothing, collision avoidance, and emergency braking. These mechanisms are essential for safe operation but suppress abrupt or unsafe commands, leading to attenuation of malicious behaviors learned in simulation.

We treat  $\mathcal{C}$  as a black-box system. The attacker cannot access, modify, or differentiate through  $\mathcal{C}$ . Accordingly, DGBA defines attack success on the executed behavior after safety filtering, as defined in Eq. 13. This ensures that both diffusion-based trigger generation and poisoning optimization are implicitly shaped to overcome real control-stack attenuation without modeling controller dynamics.

---

**Algorithm 1** DGBA Backdoor Training

---

**Require:** PPO ( $\pi_\theta, V_\phi$ ), ratio  $\beta$ , mask  $M$ , diffusion  $p_\psi$ , augmentation  $\mathcal{A}$

**Ensure:** Backdoored policy  $\pi_{\theta^*}$

- 1: Train clean PPO to get  $\theta_0$
- 2: **for** each PPO iteration **do**
- 3:   Collect rollout and compute  $A_t$
- 4:   Select top  $K = \lfloor \beta H \rfloor$  steps by  $|A_t|$
- 5:   **for** each selected step **do**
- 6:     Sample  $p_t \sim p_\psi(\cdot | x_t)$
- 7:      $p_t \leftarrow \mathcal{A}(p_t)$
- 8:      $\tilde{x}_t \leftarrow (1 - M) \odot x_t + M \odot p_t$
- 9:     Replace  $o_t$  by  $\tilde{o}_t$  and apply poisoning
- 10:   **end for**
- 11:   Update PPO parameters
- 12: **end for**
- 13: **return**  $\pi_{\theta^*}$

---

**Algorithm 2** DGBA Real-World Deployment

---

**Require:** Backdoored policy  $\pi_{\theta^*}$ , diffusion  $p_\psi$

**Ensure:** Printable trigger patch  $p^*$

- 1: Sample  $p^* \sim p_\psi$
- 2: Print and place  $p^*$  on floor
- 3: Deploy  $\pi_{\theta^*}$  with control stack  $\mathcal{C}$
- 4: Observe executed behavior  $\tilde{a}_t$

---

## 4.7 Training and Deployment Pipeline

DGBA follows a three-stage pipeline, summarized in Algorithm 1 and Algorithm 2.

Stage 1 trains a clean PPO policy  $\pi_{\theta_0}$  in simulation to obtain strong nominal navigation performance.

Stage 2 finetunes PPO starting from  $\theta_0$ . At each iteration, rollouts are collected, advantages computed, decision-critical states selected, diffusion-sampled and physically augmented patches injected, and PPO updates performed on mixed clean and poisoned data. Because poisoning is sparse and concentrated on high-leverage transitions, the learned policy preserves clean-task performance while associating the trigger with target executed behaviors under safety filtering.

Stage 3 deploys the backdoored policy  $\pi_{\theta^*}$  on TurtleBot3 without modifying the control stack. A patch instance  $p^*$  is sampled from the diffusion generator, printed, and placed on the floor. The robot perceives the patch through its onboard camera and executes

$$\tilde{a}_t = \mathcal{C}(\pi_{\theta^*}(\tilde{o}_t)). \quad (15)$$

We measure both attack success and clean-task performance under real safety-constrained control.

## 5 Experimental Setup

### 5.1 TurtleBot3 Platform and Safety-Constrained Control Stack

We evaluate DGBA on a TurtleBot3 Burger robot equipped with a forward-facing RGB camera and a 2D LiDAR sensor. The robot operates under the standard ROS navigation stack,

which enforces velocity limiting, action smoothing, and collision avoidance. Policy outputs are filtered by this safety-constrained controller before execution, and the controller remains enabled throughout all real-world experiments without modification or attacker access, reflecting realistic deployment conditions.

The robot uses an external USB RGB camera capturing  $640 \times 480$  images at 22–24 Hz, resized to  $84 \times 84$  as visual input  $x_t$ . The 2D LiDAR provides full  $360^\circ$  scans at approximately 7 Hz. Raw scans contain 360 range measurements, which are uniformly subsampled into a 36-dimensional vector  $s_t$  for policy input. Meanwhile, full-resolution LiDAR scans are consumed internally by the ROS navigation stack to perform real-time collision avoidance and emergency braking. All experiments are conducted in an indoor environment with static obstacles.

### 5.2 Navigation Task and Evaluation Protocol

The navigation task requires the robot to move from a fixed start position to a goal while avoiding obstacles. The clean policy drives the robot forward, bypasses obstacles, and reaches the goal under the safety-constrained controller. Clean-task performance is measured by the success rate of reaching the goal within a fixed time limit.

For attack evaluation, a printed trigger patch is placed before an obstacle. Without the patch, the robot avoids the obstacle and reaches the goal; with the patch, the backdoored policy executes target behaviors (left, right, straight, or stop) despite safety filtering. A single trigger  $p^*$  is sampled from the diffusion generator, exported as a printable RGB image, placed on the route, and experiments are repeated with randomized initial orientations for reliable evaluation.

### 5.3 Implementation Details

We use PPO [Schulman *et al.*, 2017] as the primary victim algorithm and additionally evaluate TRPO [Schulman *et al.*, 2015] to test cross-algorithm generalization. The policy network consists of a convolutional visual encoder processing  $3 \times 84 \times 84$  images, followed by a two-layer MLP fusing visual features with the 36-dimensional LiDAR input to produce continuous control commands. The value network shares the same visual encoder.

The diffusion-based trigger generator is a conditional U-Net [Ronneberger *et al.*, 2015] producing  $16 \times 16$  trigger patches at the policy input resolution. For deployment, patches are upsampled and exported as  $128 \times 128$  printable RGB images. All policy and diffusion training are conducted in Gazebo [Koenig and Howard, 2004] with camera and LiDAR settings matching the real robot. Trained policies are then evaluated on a physical TurtleBot3 Burger platform.

The diffusion model is trained jointly with the policy using the standard noise-prediction objective for 200 finetuning iterations. The advantage-based poisoning ratio is set to  $\beta = 0.05$ , modifying only the top 5% of decision-critical transitions. The patch mask covers a  $16 \times 16$  region in the lower part of the resized camera image, corresponding to a floor patch region in the robot’s field of view.

Physical-style augmentation includes random scaling, perspective warping, brightness and contrast jitter, color pertur-

Table 1: Main results on PPO victim under real-world deployment.

Method	CSR (%)	ASR (%)
Clean PPO (no attack)	91.1	—
TrojDRL [Kiourtzi <i>et al.</i> , 2019]	85.6	34.5
BadRL [Cui <i>et al.</i> , 2024]	87.3	57.0
SleeperNets [Rathbun <i>et al.</i> , 2024]	88.7	21.3
DGBA (ours)	<b>89.1</b>	<b>83.5</b>

bation, and partial occlusion. These augmentations are applied during finetuning and introduce moderate geometric and photometric variability. TrojDRL, BadRL, and SleeperNets are trained with the same physical-style data augmentation as DGBA.

## 6 Results

### 6.1 Main Results on PPO Victim

We first evaluate DGBA and all baselines on the PPO victim policy under real-world deployment. Each method is trained with the same poisoning budget ( $\beta = 5\%$ ), identical network architecture, data augmentation, and deployment setting. During real-world evaluation, the trained policy is deployed on the TurtleBot3 platform with the safety-constrained control stack enabled.

We report two metrics: (i) *Clean Success Rate (CSR)*, defined as the fraction of trials where the robot reaches the goal without collision in the absence of the trigger; (ii) *Attack Success Rate (ASR)*, defined as the fraction of trials where the robot executes the target behavior after observing the trigger patch.

For completeness, PPO optimizes the clipped surrogate objective

$$\mathcal{L}_{\text{PPO}}(\theta) = \mathbb{E}_t \left[ \min(r_t(\theta)A_t, \bar{r}_t(\theta)A_t) \right], \quad (16)$$

where

$$r_t(\theta) = \frac{\pi_\theta(a_t | o_t)}{\pi_{\theta_{\text{old}}}(a_t | o_t)}, \quad (17)$$

$$\bar{r}_t(\theta) = \text{clip}(r_t(\theta), 1 - \epsilon, 1 + \epsilon), \quad (18)$$

and  $A_t$  is the advantage estimate.

Table 1 summarizes the real-world performance. The clean PPO policy achieves a high success rate, indicating stable navigation under the safety-constrained controller. All backdoored policies preserve comparable clean-task performance, showing that sparse poisoning does not degrade nominal behavior.

In contrast, existing RL backdoor baselines show limited effectiveness when deployed on real robots with safety-constrained control stacks. SleeperNets [Rathbun *et al.*, 2024] yields the lowest ASR (21.3%), indicating that representation-level backdoors are sensitive to real-world visual variability and control filtering. TrojDRL [Kiourtzi *et al.*, 2019] achieves moderate attack performance (34.5%), but its fixed trigger pattern remains vulnerable to physical imaging variations. BadRL [Cui *et al.*, 2024] improves attack effectiveness by targeting decision-critical states for poisoning and

Table 2: Results on TRPO victim under real-world deployment.

Method	CSR (%)	ASR (%)
Clean TRPO (no attack)	93.4	—
TrojDRL [Kiourtzi <i>et al.</i> , 2019]	82.5	43.9
BadRL [Cui <i>et al.</i> , 2024]	88.2	46.5
SleeperNets [Rathbun <i>et al.</i> , 2024]	87.9	11.9
DGBA (ours)	<b>90.7</b>	<b>76.3</b>

reaches an ASR of 57.0%, yet its digital trigger is still susceptible to real-world visual disturbances and controller suppression.

DGBA consistently outperforms all baselines in attack success. Its high ASR of 83.5% indicates that diffusion-generated physical patch distributions produce stable trigger effects under real-world visual conditions and remain effective after safety-constrained control execution. At the same time, DGBA maintains a competitive CSR of 89.1% among all attack methods, showing that reliable backdoor activation is achieved without sacrificing nominal navigation performance.

Fig. 3 shows real-world execution sequences of clean navigation and trigger-induced behaviors on TurtleBot3. These visual results provide qualitative evidence of backdoor activation under safety-constrained real-world control.

These results confirm that addressing perception variability and control-induced attenuation is crucial for effective backdoor attacks in real-world reinforcement learning systems.

### 6.2 Results on TRPO Victim

To evaluate cross-algorithm generalization, we further test DGBA and all baselines on a TRPO victim policy under the same real-world deployment setting. All methods use identical poisoning budgets, network architectures, data augmentation, and training procedures as in the PPO experiments. All TRPO policies are evaluated on the TurtleBot3 robot under the same experimental settings.

For completeness, TRPO optimizes the trust-region surrogate objective

$$\mathcal{L}_{\text{TRPO}}(\theta) = \mathbb{E}_t \left[ r_t(\theta)A_t \right], \quad (19)$$

subject to a KL-divergence constraint

$$\mathbb{E}_t \left[ D_{\text{KL}}(\pi_{\theta_{\text{old}}}(\cdot | o_t) \| \pi_\theta(\cdot | o_t)) \right] \leq \delta, \quad (20)$$

where  $r_t(\theta)$  is the probability ratio and  $A_t$  is the advantage estimate.

Table 2 shows that the TRPO victim exhibits behavior similar to PPO, achieving high clean-task performance across all methods. Attack success rates are generally lower than PPO, reflecting TRPO’s robustness to perturbations, but DGBA still achieves the highest ASR, demonstrating effective cross-algorithm generalization.

### 6.3 Ablation Studies

We conduct ablation experiments on the PPO victim to quantify the contribution of each component in DGBA. All ablations are evaluated under identical real-world deployment

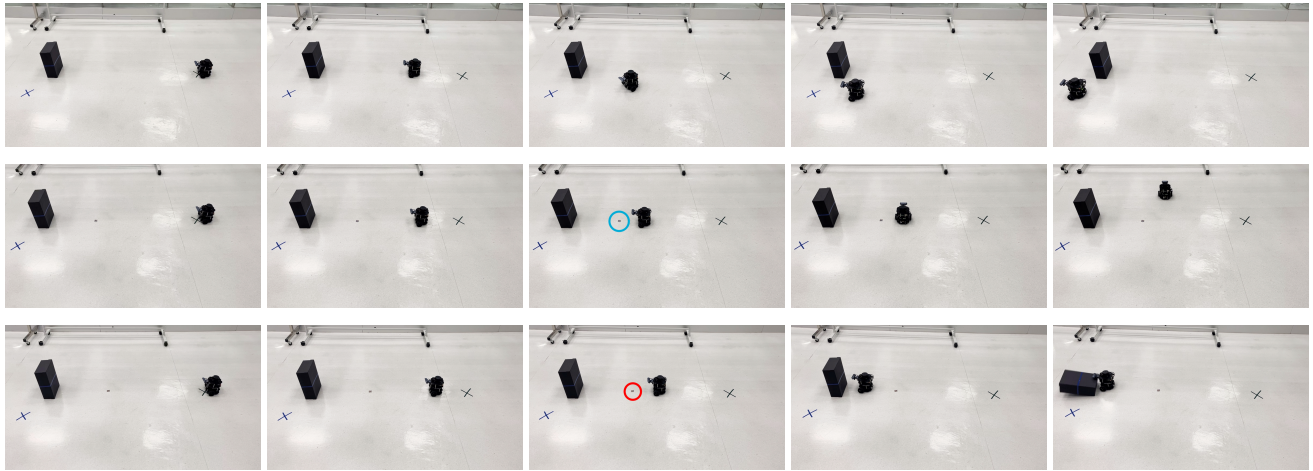


Figure 3: Real-world demonstrations on TurtleBot3. Top row: clean navigation without trigger. Middle row: trigger-activated right-turn behavior. Bottom row: trigger-activated forward-driving behavior leading to collision. Frames are shown from left to right over time.

Table 3: Ablation results on PPO victim under real-world deployment.

Method	CSR (%)	ASR (%)
DGBA (full)	89.1	83.5
w/o Diffusion	86.0	43.4
w/o Physical Augmentation	88.5	56.7
w/o Advantage Poisoning	90.2	51.6
Poisoning Rate $\beta = 5\%$	89.1	83.5
Poisoning Rate $\beta = 10\%$	87.3	88.7
Poisoning Rate $\beta = 15\%$	81.6	89.4

conditions and the same poisoning budget unless otherwise specified. Specifically, *w/o Diffusion* replaces the diffusion-based trigger generator with a single fixed patch; *w/o Physical Augmentation* disables geometric and photometric transformations during poisoning; *w/o Advantage Poisoning* replaces advantage-based state selection with uniform random poisoning. Results are reported in Table 3.

**Effect of diffusion-based trigger generation.** Removing the diffusion generator leads to a substantial drop in ASR from 83.5% to 43.4%. Without diffusion modeling, the trigger degenerates to a fixed physical patch, which is highly sensitive to viewpoint, illumination, and background texture variations. This confirms that learning a distribution of patch appearances is essential for producing stable trigger effects under real-world visual conditions.

**Effect of physical-style augmentation.** Disabling physical-style augmentation reduces ASR to 56.7%, while CSR remains comparable. This indicates that geometric and photometric perturbations introduced during training effectively improve consistency to real camera projection and lighting changes. Without such augmentation, diffusion-generated patches overfit training image statistics and produce less stable trigger activation in real-world observations.

**Effect of advantage-based poisoning.** Replacing advantage-based state selection with uniform poisoning decreases ASR

to 51.6%. This demonstrates that concentrating poisoned samples on decision-critical states substantially improves backdoor learning efficiency under limited poisoning budgets.

**Effect of poisoning rate.** We further vary the poisoning ratio  $\beta$  while keeping all other components unchanged. Increasing  $\beta$  from 5% to 10% improves ASR from 83.5% to 88.7%, indicating that additional poisoned samples strengthen the learned trigger effect. At  $\beta = 15\%$ , ASR saturates at 89.4%, while CSR drops more noticeably to 81.6%, revealing a trade-off between attack strength and clean-task performance. This trend confirms that DGBA achieves high attack success under low poisoning budgets, while excessive poisoning begins to interfere with nominal navigation behavior.

Overall, each component contributes critically to real-world backdoor effectiveness, and removing any one leads to a marked performance drop. Only their combination achieves high attack success without sacrificing clean-task performance.

## 7 Conclusion

We studied backdoor attacks in real-world reinforcement learning and showed that safety-constrained robot control stacks substantially attenuate conventional RL backdoors developed in simulation. To bridge this gap, we propose DGBA, which builds physically deployable floor-patch triggers via diffusion modeling. DGBA couples diffusion-based trigger synthesis with sparse advantage poisoning to achieve reliable targeted behaviors without degrading nominal navigation.

Real-robot experiments on TurtleBot3 demonstrate that prior RL backdoor baselines suffer severe effectiveness degradation under safety filtering, whereas DGBA consistently achieves high attack success on both PPO and TRPO victims. These findings indicate that security evaluations of RL systems must account for real-world perception and control constraints.

## References

- [Amsters and Slaets, 2019] Robin Amsters and Peter Slaets. Turtlebot 3 as a robotics education platform. In Münir Merdan, Wilfried Lepuschitz, Gottfried Koppensteiner, Richard Balogh, and David Obdrzálek, editors, *Robotics in Education - Current Research and Innovations, Proceedings of the 10th RiE, Vienna, Austria, April 10-12, 2019*, volume 1023 of *Advances in Intelligent Systems and Computing*, pages 170–181. Springer, 2019.
- [Babu and Kirchner, 2025] Ajish Babu and Frank Kirchner. Stepping locomotion for a walking excavator robot using hierarchical reinforcement learning and action masking. In *IEEE/RSJ International Conference on Intelligent Robots and Systems, IROS 2025, Hangzhou, China, October 19-25, 2025*, pages 4917–4923. IEEE, 2025.
- [Chandra *et al.*, 2025] Rohan Chandra, Haresh Karnan, Negar Mehr, Peter Stone, and Joydeep Biswas. Multi-agent inverse reinforcement learning in real world unstructured pedestrian crowds. In *IEEE/RSJ International Conference on Intelligent Robots and Systems, IROS 2025, Hangzhou, China, October 19-25, 2025*, pages 18668–18675. IEEE, 2025.
- [Chen *et al.*, 2025] Timothy Chen, Ola Shorinwa, Joseph Bruno, Aiden Swann, Javier Yu, Weijia Zeng, Keiko Nagami, Philip M. Dames, and Mac Schwager. Splat-nav: Safe real-time robot navigation in gaussian splatting maps. *IEEE Trans. Robotics*, 41:2765–2784, 2025.
- [Choi *et al.*, 2025] Jason J. Choi, Fernando Castañeda, Wonsuhk Jung, Bike Zhang, Claire J. Tomlin, and Koushil Sreenath. Constraint-guided online data selection for scalable data-driven safety filters in uncertain robotic systems. *IEEE Trans. Robotics*, 41:3779–3798, 2025.
- [Cui *et al.*, 2024] Jing Cui, Yufei Han, Yuzhe Ma, Jianbin Jiao, and Junge Zhang. Badrl: Sparse targeted backdoor attack against reinforcement learning. In Michael J. Wooldridge, Jennifer G. Dy, and Sriraam Natarajan, editors, *Thirty-Eighth AAAI Conference on Artificial Intelligence, AAAI 2024, Thirty-Sixth Conference on Innovative Applications of Artificial Intelligence, IAAI 2024, Fourteenth Symposium on Educational Advances in Artificial Intelligence, EAAI 2024, February 20-27, 2024, Vancouver, Canada*, pages 11687–11694. AAAI Press, 2024.
- [Filho *et al.*, 2025] Edson B. Ferreira Filho, David F. Brochero Giraldo, Arthur H. D. Nunes, and Luciano C. A. Pimenta. Safe radial segregation algorithm for swarms of dubins-like robots. In *IEEE International Conference on Robotics and Automation, ICRA 2025, Atlanta, GA, USA, May 19-23, 2025*, pages 3044–3050. IEEE, 2025.
- [Ho *et al.*, 2020] Jonathan Ho, Ajay Jain, and Pieter Abbeel. Denoising diffusion probabilistic models. In Hugo Larochelle, Marc'Aurelio Ranzato, Raia Hadsell, Maria-Florina Balcan, and Hsuan-Tien Lin, editors, *Advances in Neural Information Processing Systems 33: Annual Conference on Neural Information Processing Systems 2020, NeurIPS 2020, December 6-12, 2020, virtual*, 2020.
- [Hu *et al.*, 2025] Xiaoyi Hu, Qiao Sun, Bailin He, Haojie Liu, Xueyi Zhang, Chunpeng lu, and Jiangwei Zhong. Impact of static friction on sim2real in robotic reinforcement learning. In *IEEE/RSJ International Conference on Intelligent Robots and Systems, IROS 2025, Hangzhou, China, October 19-25, 2025*, pages 17107–17114. IEEE, 2025.
- [Kiourti *et al.*, 2019] Panagiota Kiourti, Kacper Wardega, Susmit Jha, and Wenchao Li. Trojdr: Trojan attacks on deep reinforcement learning agents. *CoRR*, abs/1903.06638, 2019.
- [Koenig and Howard, 2004] Nathan P. Koenig and Andrew Howard. Design and use paradigms for gazebo, an open-source multi-robot simulator. In *2004 IEEE/RSJ International Conference on Intelligent Robots and Systems, Sendai, Japan, September 28 - October 2, 2004*, pages 2149–2154. IEEE, 2004.
- [Li *et al.*, 2023] Hao Li, Jinfu Huang, Peng Jin, Guoli Song, Qi Wu, and Jie Chen. Weakly-supervised 3d spatial reasoning for text-based visual question answering. *IEEE Trans. Image Process.*, 32:3367–3382, 2023.
- [Liu *et al.*, 2025] Puze Liu, Haitham Bou-Ammar, Jan Peters, and Davide Tateo. Safe reinforcement learning on the constraint manifold: Theory and applications. *IEEE Trans. Robotics*, 41:3442–3461, 2025.
- [Mnih *et al.*, 2015] Volodymyr Mnih, Koray Kavukcuoglu, David Silver, Andrei A. Rusu, Joel Veness, Marc G. Bellemare, Alex Graves, Martin A. Riedmiller, Andreas Fidjeland, Georg Ostrovski, Stig Petersen, Charles Beattie, Amir Sadik, Ioannis Antonoglou, Helen King, Dharshan Kumaran, Daan Wierstra, Shane Legg, and Demis Hassabis. Human-level control through deep reinforcement learning. *Nat.*, 518(7540):529–533, 2015.
- [Oishi *et al.*, 2025] Koshi Oishi, Teruki Kato, Hiroya Makino, and Seigo Ito. Visual-based forklift learning system enabling zero-shot sim2real without real-world data. In *IEEE International Conference on Robotics and Automation, ICRA 2025, Atlanta, GA, USA, May 19-23, 2025*, pages 4915–4921. IEEE, 2025.
- [Rathbun *et al.*, 2024] Ethan Rathbun, Christopher Amato, and Alina Oprea. Sleepernets: Universal backdoor poisoning attacks against reinforcement learning agents. In Amir Globersons, Lester Mackey, Danielle Belgrave, Angela Fan, Ulrich Paquet, Jakub M. Tomczak, and Cheng Zhang, editors, *Advances in Neural Information Processing Systems 38: Annual Conference on Neural Information Processing Systems 2024, NeurIPS 2024, Vancouver, BC, Canada, December 10 - 15, 2024*, 2024.
- [Rengarajan *et al.*, 2022a] Desik Rengarajan, Sapana Chaudhary, Jaewon Kim, Dileep Kalathil, and Srinivas Shakkottai. Enhanced meta reinforcement learning using demonstrations in sparse reward environments. *CoRR*, abs/2209.13048, 2022.
- [Rengarajan *et al.*, 2022b] Desik Rengarajan, Gargi Vaidya, Akshay Sarvesh, Dileep M. Kalathil, and Srinivas Shakkottai. Reinforcement learning with sparse rewards using guidance from offline demonstration. In *The Tenth*

- [Rengarajan *et al.*, 2024] Desik Rengarajan, Nitin Ragothaman, Dileep Kalathil, and Srinivas Shakkottai. Federated ensemble-directed offline reinforcement learning. In Amir Globersons, Lester Mackey, Danielle Belgrave, Angela Fan, Ulrich Paquet, Jakub M. Tomczak, and Cheng Zhang, editors, *Advances in Neural Information Processing Systems 38: Annual Conference on Neural Information Processing Systems 2024, NeurIPS 2024, Vancouver, BC, Canada, December 10 - 15, 2024*, 2024.
- [Ronneberger *et al.*, 2015] Olaf Ronneberger, Philipp Fischer, and Thomas Brox. U-net: Convolutional networks for biomedical image segmentation. In Nassir Navab, Joachim Hornegger, William M. Wells III, and Alejandro F. Frangi, editors, *Medical Image Computing and Computer-Assisted Intervention - MICCAI 2015 - 18th International Conference Munich, Germany, October 5 - 9, 2015, Proceedings, Part III*, volume 9351 of *Lecture Notes in Computer Science*, pages 234–241. Springer, 2015.
- [Schulman *et al.*, 2015] John Schulman, Sergey Levine, Pieter Abbeel, Michael I. Jordan, and Philipp Moritz. Trust region policy optimization. In Francis R. Bach and David M. Blei, editors, *Proceedings of the 32nd International Conference on Machine Learning, ICML 2015, Lille, France, 6-11 July 2015*, volume 37 of *JMLR Workshop and Conference Proceedings*, pages 1889–1897. JMLR.org, 2015.
- [Schulman *et al.*, 2017] John Schulman, Filip Wolski, Prafulla Dhariwal, Alec Radford, and Oleg Klimov. Proximal policy optimization algorithms. *CoRR*, abs/1707.06347, 2017.
- [Song *et al.*, 2020] Jiaming Song, Chenlin Meng, and Stefano Ermon. Denoising diffusion implicit models. *CoRR*, abs/2010.02502, 2020.
- [Tang *et al.*, 2025] Chen Tang, Ben Abbatematteo, Jiaheng Hu, Rohan Chandra, Roberto Martín-Martín, and Peter Stone. Deep reinforcement learning for robotics: A survey of real-world successes. In Toby Walsh, Julie Shah, and Zico Kolter, editors, *AAAI-25, Sponsored by the Association for the Advancement of Artificial Intelligence, February 25 - March 4, 2025, Philadelphia, PA, USA*, pages 28698–28699. AAAI Press, 2025.
- [Wang *et al.*, 2024] Kuang-Da Wang, Yu-Tse Chen, Yu-Heng Lin, Wei-Yao Wang, and Wen-Chih Peng. The coachai badminton environment: Bridging the gap between a reinforcement learning environment and real-world badminton games. In Michael J. Wooldridge, Jennifer G. Dy, and Sriraam Natarajan, editors, *Thirty-Eighth AAAI Conference on Artificial Intelligence, AAAI 2024, Thirty-Sixth Conference on Innovative Applications of Artificial Intelligence, IAAI 2024, Fourteenth Symposium on Educational Advances in Artificial Intelligence, EAAI 2024, February 20-27, 2024, Vancouver, Canada*, pages 23844–23846. AAAI Press, 2024.
- [Zhang *et al.*, 2023] Lvmin Zhang, Anyi Rao, and Maneesh Agrawala. Adding conditional control to text-to-image diffusion models. In *IEEE/CVF International Conference on Computer Vision, ICCV 2023, Paris, France, October 1-6, 2023*, pages 3813–3824. IEEE, 2023.
- [Zhang *et al.*, 2025] Yikun Zhang, Xinxing Chen, and Jian Huang. Safe corridor-based MPC for follow-ahead and obstacle avoidance of mobile robot in cluttered environments. In *IEEE/RSJ International Conference on Intelligent Robots and Systems, IROS 2025, Hangzhou, China, October 19-25, 2025*, pages 5045–5052. IEEE, 2025.
- [Zhou *et al.*, 2023] Ruida Zhou, Tao Liu, Min Cheng, Dileep Kalathil, P. R. Kumar, and Chao Tian. Natural actor-critic for robust reinforcement learning with function approximation. In Alice Oh, Tristan Naumann, Amir Globerson, Kate Saenko, Moritz Hardt, and Sergey Levine, editors, *Advances in Neural Information Processing Systems 36: Annual Conference on Neural Information Processing Systems 2023, NeurIPS 2023, New Orleans, LA, USA, December 10 - 16, 2023*, 2023.
- [Zhu *et al.*, 2020] Henry Zhu, Justin Yu, Abhishek Gupta, Dhruv Shah, Kristian Hartikainen, Avi Singh, Vikash Kumar, and Sergey Levine. The ingredients of real world robotic reinforcement learning. In *8th International Conference on Learning Representations, ICLR 2020, Addis Ababa, Ethiopia, April 26-30, 2020*. OpenReview.net, 2020.